Journal of Photochemistry and Photobiology A: Chemistry 209 (2010) 135–146

Contents lists available at ScienceDirect

Journal of Photochemistry and Photobiology A: Chemistry

journal homepage: www.elsevier.com/locate/jphotochem

Structural changes accompanying excited-state electron transfer in *meta*- and *para*-dialkylaminopyridines

Izabela Franssen Szydłowska[a], Jacek Nowacki[b], Jerzy Herbich[a,c,*]

[a] Institute of Physical Chemistry, Polish Academy of Sciences, Kasprzaka 44/52, 01-224 Warsaw, Poland
[b] Department of Chemistry, Warsaw University, Pasteura 1, 03-093 Warsaw, Poland
[c] Faculty of Mathematics and Science, Cardinal Stefan Wyszyński University, Dewajtis 5, 01-815 Warsaw, Poland

ARTICLE INFO

Article history:
Received 10 September 2009
Received in revised form 2 November 2009
Accepted 9 November 2009
Available online 18 November 2009

Keywords:
Dialkylaminopyridines
UV–vis spectroscopy and MCD
Dual fluorescence
IET
TICT states
INDO/S
DFT and TD-DFT calculations

ABSTRACT

The electronic structure of the lowest excited singlet states and molecular geometries of a series of dialkylaminopyridines (DAAPs) representing electron donor–acceptor systems were studied by photostationary and time-resolved UV–vis spectroscopic methods and quantum chemical calculations. The comparative studies allow us to rationalize dual luminescence of 4-DAAPs in terms of the TICT state model—the analysis of the electronic transition dipole moments indicates a nearly orthogonal conformation of the fluorescent ICT states. Introduction of the amino group at *meta* position as in 3-diisopropylaminopyridine completely changes photophysics of these pyridine derivatives: (i) the Franck-Condon excited state initially reached upon excitation and the solvent equilibrated fluorescent state are most probably of the same nature (both excited states do not correspond to a full separation of charges) and (ii) the electronic structure and geometry of the fluorescent CT states of *m*-DIAP are solvent dependent.

1. Introduction

Photoinduced electron transfer (ET) reactions in donor–acceptor molecules linked by a single bond (D–A) are of particular interest for the last 40 years [1–3]. A particular attention is paid to the D–A systems showing solvent-dependent dual fluorescence from the substrate and product of excited-state ET. The most eminent example is dual luminescence of 4-(dimethylamino)benzonitrile (DMABN) discovered by Lippert et al. [1] and interpreted in terms of the twisted intramolecular charge transfer (TICT) state model by Grabowski et al. [2,3]. This model assumes that dielectric polarization of the solvent permits rotational isomerization of the substrate (the initially excited state) into the product (the highly polar TICT state) of the ET reaction with a perpendicular conformation of the D^+ and A^- subunits. Another interpretation, proposed by Zachariasse [4], postulates that the origin of the "driving force" for the excited-state electron transfer process is connected with the change of the molecular structure from the primary excited state of low-symmetry (because of a pyramidalization of the $-N(CH_3)_2$ group nitrogen atom due to a "solvent-induced pseudo-Jahn–Teller interaction" between the two lowest, closely lying, excited singlet states S_1 and S_2) to a conjugated planar ICT (PICT) state of a quinoidal structure. It should be noted that the detailed *ab initio* calculations performed by Zilberg and Haas [5], which include configuration interaction treatment, predict two low-lying excited states of CT character which are formed as a consequence of the Jahn–Teller distortion of the benzene anion radical. One of them has a quinoid structure, the other one, an anti-quinoid structure with the bond lengths of the central carbon atoms in the ring longer than those in benzene. According to the authors, for both structures rotation around the C_{phenyl}–N bond is quite easy for the amino and pyrrole derivatives. As the dipole moment is larger in the perpendicular geometry than that in the planar one, the former geometry is preferred in polar solvents, supporting the TICT model. However, in many cases the planar conformation of CT excited states is lower in energy than that of the LE states, and low-energy CT fluorescence can be observed also from planar structures [6].

An interesting class of D–A molecules is constituted by 4-dimethylaminopyridine (DMAP) [7–13], its *ortho*-methylated sterically hindered derivatives (MDMAP and TMAP) [9–11] and dialkylamino analogues (DEAP and DIAP, Fig. 1) because their chemical behaviour is strongly modified by hydrogen bonding [8,13]. The photophysical properties of DMAP fit well to the TICT model, *i.e.* the analysis of the luminescence data gives the similarly low values of the electronic transition dipole moments M_{fl} of the CT fluorescence of DMAP and its "pretwisted" *ortho*-methylated derivatives as it is expected for the π-electronic

* Corresponding author. Fax: +48 22 3433333.
E-mail address: herbich@ichf.edu.pl (J. Herbich).

1010-6030/$ – see front matter © 2009 Elsevier B.V. All rights reserved.
doi:10.1016/j.jphotochem.2009.11.006

decoupling between the orthogonal D^+ (*i.e.* dimethylamino group) and A^- (pyridine ring) subunits [10]. Moreover, the time-resolved picosecond fluorescence investigations of DMAP prove the bimodal kinetics of the excited-state ET reaction in polar solvents [12]. It is noteworthy that the N_1-protonated forms of 4-diisopropylaminopyridine (DIAP), contrary to other DAAPs, exhibit TICT fluorescence [13].

4-Dimethylaminopyridines are very interesting family of molecules because of many chemical and biochemical aspects. The compounds have been found to have general applicability as super nucleophilic catalysts [14,15]. DMAP has been recently used as a capping ligand for gold nanoparticles [16,17]. The efforts in this subject arise from the unique electronic, optical, and catalytic properties of metal nanoparticles [18], and particularly promising applications of gold nanoparticle systems in cell transfection, drug delivery and biological sensors [18–20]. Aminopyridines have also had biochemical applications as model compounds of the pyrimidine bases [21,22].

The problems referred in this paper concern the solvent-dependent relationship between the geometry, spectroscopy, photophysics and photochemistry of the series of dialkylaminopyridines, DAAPs (Fig. 1). Thus, the effects of solvent polarity on the room temperature absorption and dual luminescence as well as the quantitative characterization of the electronic structure, excited-state dipole moments, radiative and radiationless transitions and the resulting structural changes are examined and discussed. Moreover, the aim of this work is to study the effect of position (*para* vs. *meta*) of the electron donating dialkylamino substituent on the spectroscopic and photophysical properties of DAAPs. It should be noted that the photophysics of aminopyridines strongly depend on the position of the amino group [23–25]. This effect has also been observed for a series of *meta*- and *para*-substituted aniline and N,N-dimethylaniline derivatives [4,26,27]. However, the interpretation of these effects is still a subject of controversy.

2. Experimental

2.1. Materials and synthesis

4-Dimethylaminopyridine (Aldrich) was purified by crystallization from *n*-hexane. The synthesis of the other DAAPs under study has been described in Refs. [9,13]. In short, 3-methyl-4-(dimethylamino)pyridine (MDMAP) and 3,5-dimethyl-4-(dimethylamino)pyridine (TMAP) were synthesized from 3-picoline-1-oxide and 3,5-lutidine, respectively, following procedures reported elsewhere [9,28]. 4-Diethylaminopyridine (DEAP) was prepared by replacement of the labile halo group in 4-chloropyridine with diethylamine while heating in an autoclave at 150 °C [29]. The product was purified by vacuum distillation. Yield: 85%, b.p. 132–134 °C/10 Torr (Lit. [30]: 156–158 °C/19 Torr). 4-Diisopropylaminopyridine (DIAP) was obtained along with 3-diisopropylaminopyridine (*m*-DIAP) by reaction of diisopropylamine with 3,4-didehydropyridine generated by treatment of 3-bromopyridine with $NaNH_2$/*tert*-BuONa complex base [31]. Separation of the two component mixture of the product on a column of silicagel with 1:1 AcOEt–PE as eluent followed by vacuum distillation gave pure DIAP (b.p. 116 °C/1 Torr) and *m*-DIAP (b.p. 115–117 °C/2 Torr). Yield: approximately 20 and 27%, respectively. Purity of the products was confirmed by satisfactory elemental analysis [10,13]. It is worth to notice that DIAP was obtained as a sole product with approximately 60% yield when the addition of diisopropylamine to 3,4-didehydropyridine was carried out at −20 to −15° C.

The solvents used for our studies: *n*-hexane (HEX), dibutyl ether (BE), diethyl ether (EE), butyl acetate (BA), ethyl acetate (EA), dichloromethane (DCM), 1,2-dichloroethane (DCE), N,N-dimethylformamide (DMF), dimethyl sulphoxide (DMSO) and acetonitrile (ACN) were of spectroscopic or fluorescence grade (Aldrich or Merck). Butyronitrile, BN (Merck, for synthesis) was distilled successively over $KMnO_4 + K_2CO_3$, P_2O_5 and CaH_2. These aprotic polar solvents have been selected to cover a wide range of the static permittivity values ε [32]. All solvents were checked for the presence of fluorescing impurities.

2.2. Instrumentation and procedures

Absorption spectra were obtained on Shimadzu UV 2401 and Shimadzu UV 3100 spectrophotometers. Stationary fluorescence and fluorescence excitation spectra were measured on an Edinburgh FS 900 CDT fluorometer and with the Jasny multifunctional spectrofluorimetric system [33]. Quinine sulphate in 0.05 mol dm^{-3} H_2SO_4 ($\phi_f = 0.51$ [34]) and DMAP in ACN ($\phi_f = 0.017$ [10]) served as reference for fluorescence quantum yield determination. Fluorescence lifetimes were measured on an Edinburgh FL 900 CDT time-resolved fluorometer, with an estimated time resolution of about 300 ps. The time-resolved single photon counting technique was used, followed by data reconvolution using non-linear least squares fitting routine. Magnetic circular dichroism (MCD) investigations were carried out using a JASCO J-715 spectropolarimeter equipped with two home-built magnets operating up to 5.0 kG or an OLIS DSM 17 CD spectropolarimeter with a permanent magnet (magnetic field 9.2 kG). Enhancement of the MCD signal with respect to the baseline was achieved employing the procedure for registration of the spectra for two opposite direction setting of the magnetic field [35].

2.3. Quantum chemical calculations

All the quantum chemical calculations were performed using the Gaussian 98 [36] and Gaussian 03 [37] suites of programs. Ground-state geometries of molecules were obtained in the density functional theory (DFT) [38,39] approach using Becke's three parameter hybrid exchange functional method [40] and the correlation functional of Lee et al. [41], referred to as B3LYP, and the 6-31G(d,p) standard basis set. In order to obtain the global minimum, different starting geometries were used in optimizations. The optimized geometries were verified to correspond to real minima by calculating and diagonalizing the Hessian matrix and establishing the absence of imaginary frequencies. The vertical electronic transition energies, oscillator strength and transition moment directions were calculated using the time-dependent generalization of the density functional theory (TD-DFT) [42] at the levels of B3LYP/6-31G(d,p) and B3LYP/6-311++G(2d,p). The calculations also considered the presence of a solvent in terms of the Polarizable Continuum Model (PCM) [43]. Electronic transitions and dipole moments were also calculated using the semiempirical INDO/S method [44]. The latter method allowed us to compute the values of the MCD Faraday *B* terms.

3. Results and discussion

3.1. DFT calculations of the ground-state geometry

The optimized ground-state geometries of all the DAAPs under study have been obtained by DFT calculations. The ground-state geometry of DMAP and its *ortho*-methylated derivatives (MDMAP and TMAP) has been published previously [11]. The conformation of DMAP is nearly planar with a small out-of-plane pyramidalization of the $-N(CH_3)_2$ group. The results of above calculations are in a very

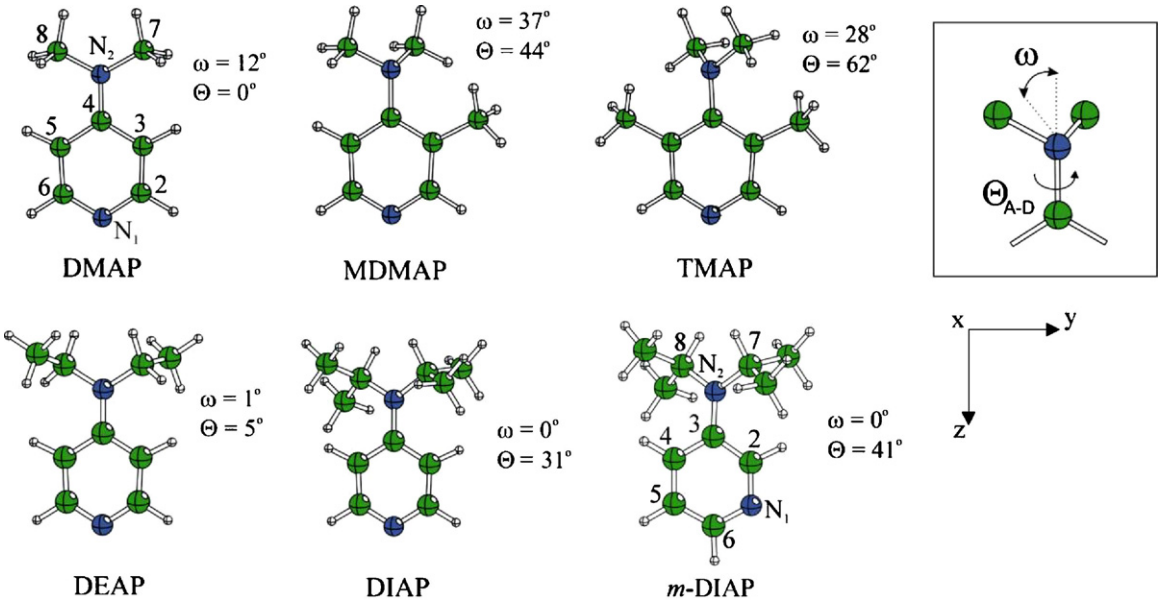

Fig. 1. Labelling of atoms and acronyms of the investigated compounds. B3LYP/6-31G(d,p) calculated ground-state molecular structures of DMAP, MDMAP, TMAP, DEAP, DIAP and *m*-DIAP. The inversion (pyramidalization) angle ω is the angle between the plane formed by the atoms C_7, C_8 and N_2 and the pyridine ring plane. The torsional angle Θ_{A-D} is defined as 0.5 (C_3–C_4–N_2–C_7 + C_5–C_4–N_2–C_8) for 4-DAAPs and as 0.5 (C_2–C_3–N_2–C_7 + C_4–C_3–N_2–C_8) for *m*-DIAP. Reproduced with permission from Ref. [13].

good agreement with X-ray crystal structure data [45]. The computed molecular structures of MDMAP and TMAP are nonplanar due to *ortho*-methylation in the pyridine ring.

The corresponding data for DEAP, DIAP and *m*-DIAP are summarized in Table 1. Two optimized geometries of DEAP were computed by the DFT method. The main difference between them is the relative conformation (*trans* and *cis*) between the two methyl groups of the diethylamino moiety. The *trans* structure, displayed in Fig. 1, seems to be a more stable form because it is 182 cm^{-1} lower in energy than the *cis* one (as computed at the B3LYP/6-31G(d,p) level of theory). The sterical hindrance resulted from relatively long alkyl chains in DEAP, DIAP and *m*-DIAP induces a twist angle Θ_{AD} of 5° for DEAP and 31° and 41° for DIAP and *m*-DIAP, respectively.

Table 1
Ground-state geometries[a] obtained by DFT calculations at the B3LYP/6-31G(d,p) level: dipole moments μ_g (in D), bond lengths (in pm), bond angles and dihedral angles (in degree).

	DEAP	DIAP	*m*-DIAP
μ_g	4.63	4.41	3.26
Bond lengths			
N_1–C_2	134.0	134.0	133.4
N_1–C_6	134.0	134.0	C_2–C_6 139.3
C_2–C_3	138.9	139.0	N_1–C_3 133.3
C_5–C_6	138.9	139.0	139.1
C_3–C_4	141.5	141.4	141.5
C_4–C_5	141.5	141.4	140.9
N_2–C_4	137.9	138.9	139.9
N_2–C_7	146.1	148.1	147.8
N_2–C_8	146.1	148.1	147.6
Bond angles			
C_2–N_1–C_6	115.0	115.1	C_2–N_1–C_3 118.0
C_3–C_4–C_5	115.0	114.9	C_2–C_3–C_4 115.5
C_7–N_2–C_8	116.7	114.3	114.7
Dihedral angles			
Θ_{A-D}[b]	5.3	31.2	41.1
ω[c]	1.0	0.3	0.2

[a] Labelling of atoms is presented in Fig. 1.
[b] The torsional angle Θ_{AD} is defined as 0.5 (C_3–C_4–N_2–C_7 + C_5–C_4–N_2–C_8) for DEAP and DIAP, and as 0.5 (C_2–C_3–N_2–C_7 + C_4–C_3–N_2–C_8) for *m*-DIAP.
[c] The inversion (pyramidalization) angle ω is defined in Fig. 1.

A negligible inversion angle is computed for the amino group in these systems ($\omega \approx 0°$). The large twist angles in DIAP and *m*-DIAP diminish the conjugation of the amino nitrogen lone pair with the pyridine ring unit and consequently increase the N_2–C_4 or N_2–C_3 bond length to 1.389 and 1.399 Å, respectively, as compared to that in DMAP (labelling of atoms is presented in Fig. 1). This bond, however, remains clearly shorter than those of MDMAP (1.414 Å) and TMAP (1.423 Å) [11].

There is no X-ray structural data published for DEAP, DIAP and *m*-DIAP. However, some structural informations about the twist and inversion angles of the donor groups in similar D–A compounds, such as 4-(diethylamino)benzonitrile (DEABN) and 4-(diisopropylamino)benzonitrile (DIABN), can be found in the literature. For DEABN, two different experimental structures have been reported. A crystal study indicates a non-twisted but slightly pyramidalized (6°) geometry [46], whereas solution phase investigations suggest that the amino group is twisted by ~21° with no pyramidalization [47]. The DFT geometry of DEAP is consistent with the results of DFT calculations on DEABN reported in Refs. [46,48] (Θ_{AD} = ~6°, ω = 0°), using the same functional and the similar basis set. The structure of DIABN obtained by X-ray spectroscopy is twisted by 14° [49] with the inversion angle ω of ~15° [50], whereas the computational study performed by Parusel et al. [46] shows, similarly to our results, the twist angle of 33° with no inversion of the amino group.

3.2. Absorption and MCD investigations

The near-UV absorption and magnetic circular dichroism (MCD) spectra of DMAP, MDMAP and TMAP have been published recently [11]. The spectra of DEAP, DIAP and *m*-DIAP recorded in *n*-hexane and acetonitrile solutions are compared with those of DMAP in Fig. 2. The INDO/S computed transition energies and MCD *B* terms are also included in the figure. The near-UV absorption spectrum of DMAP in *n*-hexane shows a shoulder between 34,000 and 36,500 cm^{-1} and a dominant band centered at 39,900 cm^{-1}. These bands reveal a red shift with increasing solvent polarity and have been previously assigned to the $^1L_b \leftarrow S_0$ and $^1L_a \leftarrow S_0$ transitions, respectively [7,11]. The MCD spectrum shows a positive *B* term for the former, and a negative *B* term for the latter (it should be stressed

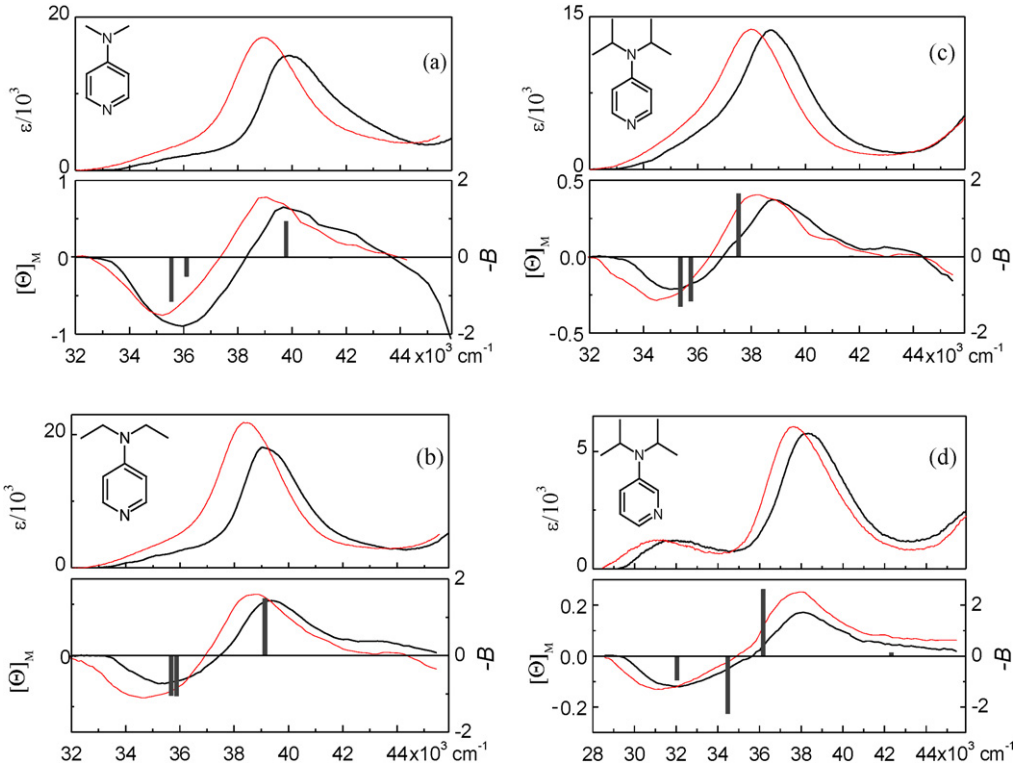

Fig. 2. Room temperature absorption (top) and MCD spectra (bottom) of DMAP (a), DEAP (b), DIAP (c) and *m*-DIAP (d) in *n*-hexane (solid lines, in black) and acetonitrile (dashed lines, in red). INDO/S calculated transition energies and *B* term values are indicated by bars. Molar absorption coefficients ε and Faraday *B* terms are given in units of $dm^3\ mol^{-1}\ cm^{-1}$ and of $10^{-3}\ \beta_e D^2$ cm [52], respectively. (For interpretation of the references to color in this figure legend, the reader is referred to the web version of the article.)

that a positive value of the *B* term corresponds to a negative MCD sign, and *vice versa*). Similar absorption spectra as those of DMAP are observed for DEAP and DIAP. The dominant absorption bands, however, in the latter compounds are shifted to lower energies by about 700 and 1300 cm^{-1}, respectively, in both *n*-hexane and acetonitrile. An analogous bathochromic shift (of about 1200 cm^{-1}) of the absorption band maximum with respect to that of DMABN was reported for DIABN [50]. The MCD spectra of DEAP and DIAP, similarly to that of DMAP, show the same, positive and negative, sequence of *B* terms. The overall MCD intensity decreases from DMAP *via* DEAP to DIAP. By comparison with DMAP, and on the basis of the spectral position, absorption intensity and solvent shift, the lowest-energy transitions observed in the MCD spectra of DEAP and DIAP are assigned to the final ^1L_b excited states in Platt's notation, whereas the next higher-energy band is attributed to the $^1L_a \leftarrow S_0$ transition.

The absorption spectrum of *m*-DIAP (Fig. 2) in *n*-hexane displays a different spectral pattern than that of the DAAPs substituted at the position 4. Compared with DIAP, a new low-energy band at 31,850 cm^{-1} arises. The second band of higher intensity, similar to that of DIAP, is located at 38,400 cm^{-1}. The spectral position of these absorption bands depends on solvent polarity—both bands in acetonitrile are red-shifted by about 700 cm^{-1} with respect to those in *n*-hexane. The MCD spectrum of *m*-DIAP shows a positive and negative sequence of the *B* terms.

The interpretation of the MCD spectra of all the DAAPs under study seems to be possible in terms of a simple perimeter model [51,52]. In the case of DMAP, DEAP, DIAP and *m*-DIAP, which contain strong-E (electron donating) substituent, the energy splitting between the two highest occupied π orbitals (ΔHOMO) is greater than that between two lowest unoccupied frontier π orbitals, ΔLUMO (Table 2). Thus, similarly to 4-aminopyridine and 3-aminopyridine [53], the +,– sequence of signs of the *B* terms corresponding to the ^1L_b and ^1L_a states is observed (Fig. 2). The nonplanar structure of MDMAP and TMAP, caused by *ortho*-methylation in the pyridine ring, is expected to result in the weakening of the substituent effect. For MCD such a result implies that the intensity should decrease with twisting of the dialkylamino group, which is indeed observed (*cf.* Figs. 5 and 6 in Ref. [11]).

Table 2
Calculated energy differences (in eV) between the two highest occupied π molecular orbitals (ΔHOMO) and the two lowest unoccupied π molecular orbitals (ΔLUMO) involved in the $^1L_b \leftarrow S_0$ and $^1L_a \leftarrow S_0$ transitions.

	DMAP*	MDMAP*	TMAP*	DEAP**	DIAP**	*m*-DIAP**
INDO/S						
ΔHOMO	0.99	0.54	0.32	1.11	1.07	1.71
ΔLUMO	0.15	0.18	0.22	0.14	0.19	0.21
TD-B3LYP/6-31G(d,p)						
ΔHOMO	1.13	0.83	0.77	1.20	1.25	1.93
ΔLUMO	0.08	0.20	0.41	0.16	0.07	0.12

* Ref. [11].
** This work.

Table 3
Comparison between INDO/S calculated energies ($\tilde{\nu}_{INDO}$, in 10^3 cm^{-1}, the energy of the $^1(n,\pi^*)$ excitations is most probably underestimated [54]) and oscillator strengths (f), corresponding to the transitions to low-lying excited singlet states S_i, and locations of MCD bands ($\tilde{\nu}_{MCD}$, in 10^3 cm^{-1}) and absorption coefficients (ε, in dm^3 mol^{-1} cm^{-1}) of the near-UV absorption band maxima in *n*-hexane.

Compound	INDO/S[a]							Experimental	
		$\tilde{\nu}_{INDO}$	f	pol[b]	μ[c]	MEC[d]		$\tilde{\nu}_{MCD}$	ε
DMAP[*]	S_0				3.7				
	S_1	35.54	0.012	12(x)	0.6	H-2 → L	$^1(n,\pi^*)$		
	S_2	36.10	0.004	y	6.0	[e]	^1L_b	36.0	
	S_3	39.78	0.376	z	8.6	H → L	^1L_a	39.9	15,600
MDMAP[*]	S_0				3.1				
	S_1	34.67	0.011	17(x)	1.2	H-2 → L	$^1(n,\pi^*)$	38.0	
	S_2	36.35	0.014	65(y)	4.1	[e]	^1L_b	36.0	
	S_3	39.88	0.172	7(z)	9.7	H → L	^1L_a	~40.0	7,900
TMAP[*]	S_0				3.1				
	S_1	34.13	0.010	18(x)	1.1	H-2 → L	$^1(n,\pi^*)$	35.3	
	S_2	35.95	0.012	15(y)	3.9	[e]	^1L_b	~34.3	
	S_3	37.27	0.084	8(z)	11.5	H → L	^1L_a	37.6	4,000
DEAP[**]	S_0				3.9				
	S_1	35.68	0.006	6(y)	5.6	[e]	^1L_b	35.6	
	S_2	35.88	0.009	x	0.8	H-2 → L	$^1(n,\pi^*)$		
	S_3	39.13	0.408	z	8.9	H → L	^1L_a	39.2	18,100
DIAP[**]	S_0				3.4				
	S_1	35.37	0.007	10(x)	1.7	H-2 → L	$^1(n,\pi^*)$		
	S_2	35.75	0.005	25(y)	3.9	H → L+1	^1L_b	35.3	
	S_3	37.52	0.329	z	9.7	H → L	^1L_a	38.6	13,500
m-DIAP[**]	S_0				2.6				
	S_1	32.03	0.039	41(y)	3.1	[f]	$(\pi,\pi^*)/(n,\pi^*)$	32.0	2,100
	S_2	34.48	0.052	45(x)	3.5	[g]	$(\pi,\pi^*)/(n,\pi^*)$		
	S_3	36.18	0.236	7(z)	7.0	H → L+1	$^1(\pi,\pi^*)$	37.9	9,000

[a] B3LYP/6-31G(d,p) optimized conformations used as input geometries.
[b] The angle (in degrees) between the transition dipole moment and a molecular axis given in parentheses. For values smaller than 5°, a "pure" polarization along a given axis is assumed. See Fig. 1 for the definition of axes.
[c] Dipole moments in debyes, D.
[d] Main electronic configurations, H = HOMO, L = LUMO.
[e] This transition arises mainly from the H → L+1 and H-1 → L excitations.
[f] This transition arises mainly from the H → L and H-2 → L excitations.
[g] This transition arises mainly from the H → L, H-1 → L and H-2 → L excitations.
[*] Ref. [11].
[**] This work.

For the second $^1(\pi,\pi^*)$ state the perimeter model predicts vanishing MCD intensity when ΔHOMO = ΔLUMO. Therefore, for the case of ΔHOMO ≈ ΔLUMO, the sign of the *B* term for this transition may easily be related to factors neglected in the perimeter model, such as interaction with a nearby $^1(n,\pi^*)$ state. An evidence for the existence of such a $^1(n,\pi^*)$ transition was provided by the finding of three bands in the low energy region of the MCD spectra of both MDMAP and TMAP [11]. INDO/S (Table 3) and TD-DFT (Tables SI1 and SI2 in Supporting Information) calculations confirm this result, predicting at least three transitions to lie in the low energy region. It is noteworthy that for DMAP, DEAP and DIAP the INDO/S predicted sign of the $^1(n,\pi^*)$ transition (Fig. 2; Table 3) is the same as for the lowest $^1(\pi,\pi^*)$ excitation. That would explain why the former is not detected in these compounds. Another reason may be a stronger intensity of the $^1(\pi,\pi^*)$ transitions in the MCD spectra of DMAP, DEAP and DIAP with respect to the *ortho*-methylated compounds.

The INDO/S calculations of DAAPs show the very similar pattern of low-energy transitions (Table 3) and reveal a strongly mixed character, $^1(\pi,\pi^*)$ and $^1(n,\pi^*)$, of the two lowest energy transitions. This is reflected in similar oscillator strengths and dipole moments.

The mixed character of the low energy transitions in DAAPs is corroborated by the TD-DFT calculations at the levels of B3LYP/6-31G(d,p) (Table 1SI) and B3LYP/6-311++G(2d,p) (Table 2SI). The $^1(\pi,\pi^*)$ transitions in 4-DAAPs are mainly represented by the HOMO → LUMO or HOMO → second LUMO excitations (Fig. SI1 in Supporting Information), but with a significant contamination of several other configurations. The second HOMO orbital is of σ character, localized mainly on the pyridine ring nitrogen atom. Thus, the lowest $^1(n,\pi^*)$ transitions are dominated by the second HOMO → LUMO and second HOMO → second LUMO excitations. In agreement with the experimental findings, the calculations predict the bathochromic shift of the lowest energy transitions in DEAP and DIAP as well as the lowering of the energy gap $\Delta E(^1L_b, ^1L_a)$ in DIAP, when compared with DMAP. Similar effects were observed for MDMAP and TMAP [11].

The TD-DFT calculations of *m*-DIAP suggest, that the first absorption band (Fig. 2) comprises a single electronic transition of essentially $^1(\pi,\pi^*)$ character. The second $^1(\pi,\pi^*)$ transition is separated from the first one by about 5000 cm^{-1}. The ratio between the calculated oscillator strengths of the lowest $^1(\pi,\pi^*)$ transitions is similar to that related to the measured molar absorption coefficients of the near-UV absorption bands maxima. Both excited states involve a charge transfer from the donor (diisopropylamino group) to the acceptor moiety.

It is noteworthy that when going from the 6-31G(d,p) to the more extended 6-311++G(2d,p) basis set, the calculated ordering of the ^1L_b and ^1L_a states remains unchanged, but the transition energies (Table 2 SI) are in better agreement with the experimental values. In addition, the transitions from the donor to the Rydberg-like diffuse orbitals appear in the low-energy region for all the studied compounds. Such low-lying Rydberg-like states have been reported for aminosubstituted phthalides [55]. A Rydberg-like

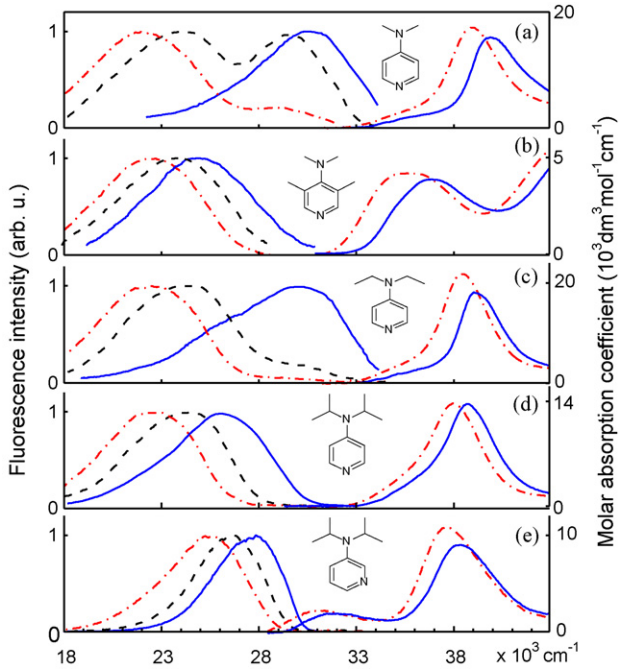

Fig. 3. Room temperature absorption and corrected and normalized fluorescence spectra of DMAP (a), TMAP (b), DEAP (c), DIAP (d) and *m*-DIAP (e) in *n*-hexane (solid lines, in blue), ethyl acetate (dashed lines, in black) and acetonitrile (dash-dotted lines, in red). The fluorescence spectra of MDMAP are very similar to those of TMAP [10]. Concentrations of the compounds were in the range from 10^{-5} to 10^{-4} mol dm^{-3}. (For interpretation of the references to color in this figure legend, the reader is referred to the web version of the article.)

character of the higher excited states in alkylaminobenzonitriles was postulated by Rotkiewicz et al. [56,57].

3.3. Fluorescence in aprotic solvents

The effects of solvent polarity on the room temperature fluorescence spectra of all the studied DAAPs are presented in Fig. 3. As reported previously [7–13], DMAP shows dual fluorescence in polar media at room temperature. In ethyl acetate (EA) the intensity of both emission bands, the high-energy *b* and the low-energy *a* (Fig. 6), is comparable [10]. Similar to DMABN [1], a considerable red shift of band *a* and the increase of its relative intensity is observed with increasing polarity of the surrounding medium. These solvent effects suggest the charge transfer character of the emitting state A* (see Section 3.4). The CT emission is dominant in highly polar solvents. On the contrary, in nonpolar solvents a dominant band *b* of low intensity is observed. This emission is attributed to the locally excited (LE) state B*.

When the –NMe$_2$ donor group in DMAP is replaced by the –NEt$_2$ group, the characteristic emission feature of DMAP is reproduced, but with a remarkable preference for the CT emission in DEAP. Even in nonpolar solvents the shape of the emission spectra suggests dual luminescence. The main short-wavelength part of the fluorescence spectrum of DEAP in *n*-hexane is attributed to the primary excited B* state of the dominant $^1(\pi,\pi^*)$ character. The shoulder between 23,000 and 28,000 cm^{-1} is probably due to the emission from the closely-lying A* state with a strong contribution of CT character. The results of INDO/S (Table 3) and TD-DFT (Tables SI1 and SI2) calculations suggest, however, that the wave functions of the fluorescent B* and A* states in nonpolar media are most probably of the mixed $^1(n,\pi^*)$, $^1(\pi,\pi^*)$ and CT character.

DIAP, contrary to DMAP and DEAP, and similarly to the other nonplanar compounds MDMAP and TMAP [9,10], emits a single fluorescence band in all the aprotic solvents. The considerable red shift of the emission and the increase of the Stokes shift with increasing solvent polarity point to the CT character of the fluorescent states of this molecule in sufficiently polar media. The shapes and positions of the fluorescence maxima of MDMAP, TMAP and DIAP match well to those of the long-wave band *a* of DMAP and DEAP in the corresponding polar solvents (Table 5). This finding suggests similar electronic structure and geometry of the solvent equilibrated CT fluorescent states. The spectra are very broad, the emission bandwidth (FWHM) of about 6200 (±500) cm^{-1} is nearly independent of solvent properties. This result, according to Marcus theory of electron transfer [58], suggests a large contribution of the inner reorganization energy (associated with the changes of the solute geometry) to the CT fluorescence profile. Thus, significant conformational changes accompanying the excited-state electron transfer are expected for the compounds.

The assignment of the fluorescence spectra of DIAP in *n*-alkanes and in low-polarity media, similarly to MDMAP and TMAP [10], is more ambiguous than that in highly polar solvents. The compounds show a single emission band strongly red-shifted with respect to that of DMAP. Most probably, the band predominantly consists of the CT emission. The origin of the red shift is analogous to that in DMABN and its derivatives and could be related to a steric hindrance to coplanarity and to the shape of the resulting ground and excited-state potential energy hypersurfaces (*cf.* Fig. 2 in Ref. [2]). Moreover, the spectra in *n*-hexane are very broad, with a FWHM value of about 6000 cm^{-1}. A strong overlap of the dual luminescence can be proposed to explain this finding. However, low-temperature experiments performed for MDMAP and TMAP in butyronitrile in the temperature range between 123 and 293 K do not show any distinct evidence for the dual luminescence [10]. This finding is most probably due to a very small, if any, barrier to the excited-state ET reaction in nonplanar 4-DAAPs (Fig. 6). This explanation is supported by the laser induced fluorescence investigations of DIAP isolated under supersonic jet conditions [59]. The position and shape of fluorescence of jet-cooled DIAP depends on excitation. The dispersed emission spectrum, recorded upon excitation in the origin region is similar to that of DMAP and DEAP and its maximum intensity is centred at 30,600 cm^{-1}. The spectrum is attributed mostly to the radiative transition from the locally excited state B*. The higher energy excitation (with excess energy of about 800 cm^{-1}) directly populates the CT state and a long-wave emission appears.

An interesting result is provided by the increase of the relative CT fluorescence intensity in 4-DAAPs resulting from the change of the dialkyl substituents in the donor group from dimethyl – *via* diethyl – to diisopropyl. The similar effects have been reported for DMABN and its analogues, DEABN [60–62] and DIABN [50], as well as for 4-dialkylaminopyrimidines [63]. It is most probably kinetic effect, *i.e.* the enhancement of the efficiency of the ICT state formation due to the lowering of the activation barrier to the excited-state charge separation process by the respective change of the donor group can be proposed to explain this finding. This hypothesis agrees with the results of MCD investigations and INDO/S (Table 3) as well as TD-DFT computations (Table SI2). The results show the decrease of the energy gap between the two lowest $^1(\pi,\pi^*)$ states, ^1L_b (of lower polarity) and ^1L_a (the latter being a precursor of the ICT state) in DIAP and DEAP with respect to DMAP. On the other hand one cannot exclude thermodynamic factors which could favor the excited-state ET reaction (*e.g.*, the less negative reaction entropies upon increasing the molecular volume) [3,61,62].

It was noticed previously that the photophysics of aminobenzonitriles [4,26] and ethyl (dimethylamino)benzoate derivatives [26] strongly depends on the position (*para* vs. *meta*) of the electron donating substituent. For example, 3-(dimethylamino)benzonitrile (*m*-DMABN) [26], contrary to DMABN, showed only a single emission band of relatively high intensity and its decay was

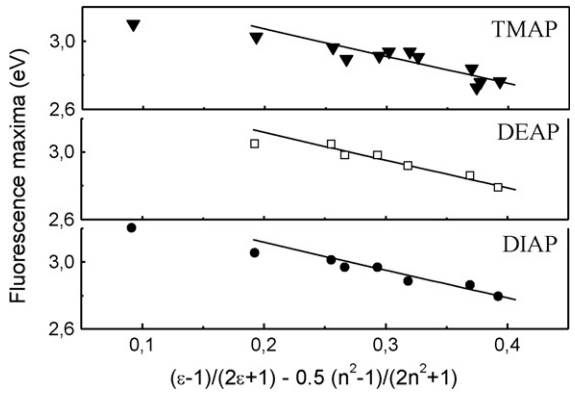

Fig. 4. Solvatochromic shift of the CT fluorescence maxima of TMAP, DEAP and DIAP in HEX, BE, EE, BA, EA, MTHF, DCM, DCE, BN, DMSO, DMF and ACN (from left to right). Correlations do not take into account the results in HEX and BE (see text for explanation).

monoexponential. Similarly, *m*-DIAP reveals a single, relatively narrow (FWHM of about 4000 cm^{-1}) fluorescence band, which is shifted to lower energies with increasing solvent polarity (Fig. 3). The shift, however, is significantly smaller than that observed for DIAP and other 4-DAAPs. This result suggests the lower dipole moment value of the fluorescent state of *m*-DIAP with respect to the CT state of 4-dialkylaminopyridines.

3.4. Excited-state dipole moments

The CT character of the fluorescent state A^* (Fig. 6) of 4-dialkylaminopyridines is verified by estimation of its dipole moment by the fluorescence solvatochromic shift method with the use of simplified Lippert–Mataga relation neglecting the mean solute polarizability in the states involved in the transition [64,65]:

$$hc\tilde{\nu}_{fl} = hc\tilde{\nu}_{fl}^{vac} - \frac{2\vec{\mu}_e(\vec{\mu}_e - \vec{\mu}_g)}{a_0^3}\left[\frac{\varepsilon - 1}{2\varepsilon + 1} - \frac{1}{2}\frac{n^2 - 1}{2n^2 + 1}\right] \quad (1)$$

where $hc\tilde{\nu}_{fl}$ and $hc\tilde{\nu}_{fl}^{vac}$ are the energies corresponding to the spectral positions of the CT fluorescence maxima in solutions and to the value extrapolated to the gas-phase, respectively, a_0 is the effective radius of the Onsager cavity [66], ε is the static dielectric constant, and n is the refractive index of a solvent.

The linear correlation of the solvent equilibrated CT fluorescence maxima $\tilde{\nu}_{fl}^{CT}$ vs. solvent polarity function, $f(\varepsilon,n)$, relates the measured quantities to the ground ($\vec{\mu}_g$) and excited-state ($\vec{\mu}_e$) dipole moments. The correlation (Fig. 4) allows one to determine directly the values of $\vec{\mu}_e(\vec{\mu}_e - \vec{\mu}_g)/a_0^3$ and to estimate the values of $\vec{\mu}_e$ under the assumption that $\vec{\mu}_e$ is parallel to $\vec{\mu}_g$ and with the radius of Onsager spherical cavity evaluated from the DFT computed dimensions of the compounds (Table 4). The obtained values of the dipole moments of the fluorescent state A^* of DMAP, DEAP and DIAP correspond to an electron transfer distance of 0.28 nm and roughly agrees with the distance between the amino nitrogen N_2 (Fig. 1) and the centre of the acceptor ring. It can be concluded from these results that the strongly red-shifted fluorescence band *a* (Fig. 6) originates indeed from a CT state, with a full electron transfer from the donor (*i.e.* the lone pair orbital on the amino nitrogen N_2) onto the π-electronic system of the acceptor ring for these molecules. This result is consistent with a radical ion pair description of the TICT state.

It is noteworthy, that the correlation between $hc\tilde{\nu}_{fl}^{CT}$ and $f(\varepsilon, n)$ for DIAP (as well as for *m*-DIAP), similarly to MDMAP and TMAP [10], is not linear in all solvents; a significant deviation from the linearity in *n*-hexane and in aprotic solvents of low-polarity is observed (Fig. 4). This finding suggests strong interactions between the lowest ^{1}CT state and a closely-lying excited state of different nature. The data collected in Table 5 and in Ref. [10] show very efficient radiationless deactivation of all the studied DAAPs in *n*-hexane and low-polarity solvents. This finding is most probably the manifestation of a strong contribution of the $^1(n,\pi^*)$ character to the wave function of the fluorescent state in low-polarity media and of a fast internal conversion (IC) to the ground state [68]. It should be noted that this efficient radiationless depopulation channel is not connected with an intersystem crossing to a close lying triplet state. The room temperature transient absorption investigations of DMAP performed by Testa [69,70] do not show any evidence of the efficient population of the triplet manifold in a nonpolar environment. Recently Demeter et al. [71] reported that the triplet yield (Φ_{ISC}) value of DMAP in ACN ($\Phi_{ISC} \cong 0.66$) is significantly higher than that in *n*-hexane, $\Phi_{ISC} \cong 0.18$. The hypothesis of the strong interactions of the lowest excited ^{1}CT state with a close-lying $^1(n,\pi^*)$ state is supported by previous studies of aminopyridines (APs) [23,25]. The very small values of the radiative rate constants ($k_f \cong 10^4 - 10^5 s^{-1}$) for 4-AP has been explained by the $^1(n,\pi^*)$ character of the fluorescent state. Thus, the analysis of the solvatochromic effects on the CT fluorescence maxima of DIAP, similarly to MDMAP and TMAP [10], has been performed in all the aprotic polar solvents excluding BE and EE.

The estimated excited-state dipole moment of the solvent-equilibrated fluorescent state of *m*-DIAP ($\mu_e \cong 8.9$ D) is considerably larger than $\mu_g \cong 3.3$ D (Table 4), clearly indicating a charge transfer from the donor to the acceptor moiety. However, the value of μ_e is smaller than the dipole moments of all the studied 4-dialkylaminopyridines and corresponds to the excited state of a partial CT character. Moreover, the long-wave absorption band of *m*-DIAP (Figs. 2 and 3) is related to a transition to the excited Franck-Condon (FC) state with a dipole moment value of about 9.3 D. This value is estimated from the dependence of the absorption maxima on the solvent polarity:

$$hc\tilde{\nu}_{abs} = hc\tilde{\nu}_{abs}^{vac} - \frac{2\vec{\mu}_g(\vec{\mu}_e - \vec{\mu}_g)}{a_0^3}\left[\frac{\varepsilon - 1}{2\varepsilon + 1} - \frac{1}{2}\frac{n^2 - 1}{2n^2 + 1}\right], \quad (2)$$

where $\tilde{\nu}_{abs}$ and $\tilde{\nu}_{abs}^{vac}$ are the spectral positions of the absorption maxima in solutions and in the gas-phase, respectively, and h is the Planck constant.

Most probably the electronic structure of the fluorescent state of *m*-DIAP is similar to that of the FC excited state reached in absorption. According to the results of the TD-DFT calculations (Tables SI1 and SI2; Fig. SI1) the latter state corresponds essentially to the $^1(\pi,\pi^*)$ excitation and involves a substantial charge redistribution with respect to the ground state.

Table 4
Ground-state ($\vec{\mu}_g$) and excited-state ($\vec{\mu}_e$) dipole moments of the studied dialkylaminopyridines.

Compound	$\vec{\mu}_g$ [D]	$\vec{\mu}_e(\vec{\mu}_e - \vec{\mu}_g)/a_0^3$ [eV]	a_0[a] [10^{-10} m]	$\vec{\mu}_e$ [D]
DMAP*	4.2[b]	1.45	3.8	13.6
DEAP**	4.6[c]	1.11	3.95	13.0
DIAP**	4.4[c]	1.02	4.1	13.0
m-DIAP**	3.3[c]	0.45	4.1	8.9

[a] The values of the Onsager's radial cavity radius were estimated from the molecular dimensions of the compounds corresponding to the B3LYP/6-311G(d,p) optimized geometry.
[b] The experimental value [67].
[c] The values calculated by DFT method at the B3LYP/6–31G(d,p) level.
* Ref. [7].
** This work.

Table 5
Solvent effects on the spectral position of the absorption ($\tilde{\nu}_{abs}$) and fluorescence maxima ($\tilde{\nu}_{fl}$), quantum yields (Φ_f), decay times (τ), and resulting radiationless (k_{nr}) and radiative (k_f) rate constants, and electronic transition dipole moments M_{fl} corresponding to the CT fluorescence for DMAP, MDMAP, TMAP, DEAP, DIAP and *m*-DIAP.

Compound	Solvent	$\tilde{\nu}_{abs}$ [cm^{-1}]	$\tilde{\nu}_{fl}$ [cm^{-1}][a]	Φ_f [b]	τ [ns]	k_{nr} (10^8 s^{-1})	k_f (10^6 s^{-1})	M_{fl}[D][f]
DMAP*	HEX[c]	39,900	30,500	~0.0015	0.08[d]	~125	~18.8	~0.9
	BE[c]	39,700	30,000					
	EA	39,400	23,500	0.014	3.1[e]			
	BN	39,000	22,700	0.016				
	ACN	38,900	21,900	0.017	3.7	~2.7	~4.6	~0.75
MDMAP**	HEX	39,100	24,900	0.004	0.95	10.5	4.2	0.6
	BE	38,900	24,200	0.015	1.9	5.2	7.9	0.8
	EA	38,600	23,500	0.020	3.6	2.7	5.6	0.7
	BN	38,000	22,800	0.019	4.3	2.3	4.4	0.7
	ACN	37,900	22,300	0.016	4.1	2.4	3.9	0.7
TMAP**	HEX	36,850	25,000	0.004	0.75	13.3	5.3	0.6
	BE	36,600	24,400	0.009	1.6	6.2	5.6	0.7
	EA	36,200	23,500	0.011	3.1	3.2	3.5	0.6
	BN	35,600	22,900	0.014	4.0	2.5	3.5	0.6
	ACN	35,400	22,300	0.012	3.9	2.5	3.1	0.6
DEAP***	HEX[c]	39,200	30,000	~0.007	~0.6	~16.5	~11.7	~0.7
	BE	38,900	24,550	0.015	1.5	6.5	10.0	0.9
	EA	38,800	24,000	0.026	4.1	2.4	6.3	0.7
	BN	38,550	23,000	0.026	4.7	2.1	5.5	0.7
	ACN	38,400	22,200	0.024	4.8	2.0	5.0	0.8
DIAP***	HEX	38,600	25,800	0.010	1.8	5.5	5.5	0.6
	BE	38,460	24,200	0.016	3.3	3.0	4.8	0.6
	EA	38,300	23,900	0.015	3.4	2.9	4.4	0.6
	BN	38,080	22,800	0.017	3.9	2.5	4.4	0.7
	ACN	38,050	22,500	0.019	4.2	2.3	4.5	0.7
m-DIAP***	HEX	31,850	27,250	0.050	1.1	8.6	45.5	1.7
	BE	31,770	26,780	0.071	1.7	5.5	41.8	1.6
	EA	31,450	26,300	0.115	3.6	2.4	31.9	1.5
	BN	31,230	25,600	0.130	5.5	1.6	23.6	1.3
	ACN	31,200	25,000	0.130	7.4	1.2	17.6	1.2

[a] Scatter of results: ±150 cm^{-1}.
[b] Error is about 10%. Thus, the maximum error is about 20% for the rate constants k_{nr} and k_f and about 10% for the transition moment M_{fl}.
[c] The parameters correspond to the primary excited fluorescence.
[d] Ref. [58].
[e] The long component of the decay time of the short-wave fluorescence is 3.2 ns (Ref. [10]).
[f] In debyes, D.
* Refs. [7,10] and this work.
** Ref. [10].
*** This work.

3.5. Electronic transition dipole moments

The challenging problem concerns the conformation of DAAPs in the fluorescent CT states. In order to gain more insight into the electronic structure and geometry of these states, solvent effects on the spectral position of the fluorescence maxima, quantum yield (Φ_f) and decay times were examined. The fluorescence data of DAAPs in solvents of various polarity are collected in Table 5. The presented results show a significant difference between the emission efficiency of *m*-DIAP and that of DIAP (and other 4-DAAPs). The Φ_f values of the CT fluorescence of all the studied 4-DAAPs are very similar, *i.e.* they are about 0.01–0.02 in aprotic polar solvents. Contrary to that, the Φ_f values of *m*-DIAP are roughly an order of magnitude higher in the respective solvents; the Φ_f values of 0.13 suggest a different character of the emitting state. More information about the nature of the radiative transitions one can obtain from the analysis of the solvent-dependence of the radiative rate constants k_f and the electronic transition dipole moments M_{fl} (being the best quantitative measure of the transition probability).

In the electric dipole approximation, the M_{fl} values of the CT fluorescence can be determined applying a simple kinetic model of an irreversible excited ^{1}CT state formation (assuming 100% efficiency). This model has been applied for the molecules which show a dominant CT emission band (*e.g.*, for DMAP and DEAP in sufficiently polar solvents). Within this model the radiationless (k_{nr}) and radiative (k_f) rate constants are simply related to the CT emission quantum yields (Φ_f) and lifetimes (τ):

$$k_{nr} = \frac{1 - \Phi_f}{\tau}, \tag{3}$$

$$k_f = \frac{\Phi_f}{\tau}, \tag{4}$$

and the resulting values of M_{fl} are given by [72,73]:

$$k_f = \frac{64\pi^4}{3h}(n\tilde{\nu}_{fl})^3|\vec{M}_{fl}|^2. \tag{5}$$

Interesting results are provided by the very similar values of M_{fl} for all the 4-DAAPs under study and the finding that M_{fl} values for MDMAP and TMAP [10], as well as DIAP and DEAP, are roughly constant in all the polar solvents. These findings suggest that the electronic structure and molecular conformation of the CT fluorescent states of 4-DAAPs do not change significantly with the change of the donor group and with solvent polarity as well as with the change of the ground-state geometry. The lack of influence of the steric hindrance on the luminescence properties of the 4-DAAPs and the low values of the electronic transition dipole moments corresponding to the CT fluorescence indicate a small overlap between the π-orbitals of the donor (*i.e.* the lone pair orbital on the amino nitrogen) and the acceptor (*i.e.* the pyridine ring). This suggests that the results can be interpreted in terms of the TICT

state model. The analysis can be performed in terms of the Mulliken [74,75] and Murrell [76] theory, which assumes that the M_{fl} values are mainly determined by the direct interactions between the lowest ^{1}CT state and the Franck-Condon ground state, and by the contributions from the locally excited configurations [77–79]. The independence of the M_{fl} values on solvent polarity, most probably due to the large energy gap between the fluorescent ^{1}CT state and the lowest $^1(\pi,\pi^*)$ state of the pyridine subunit (which lies about 38,000–39,000 cm^{-1}) [51,80], allows one to neglect the latter contributions. Thus, the M_{fl} values can be estimated from a simple relation [74,75]:

$$M_{fl} \approx \frac{V_0(\vec{\mu}_e - \vec{\mu}_g)}{hc\tilde{\nu}_{fl}} \quad (6)$$

where V_0 is the electronic coupling element between the ^{1}CT state and the ground state and c is the speed of light in a vacuum. With $\mu_e - \mu_g \cong 8.3(\pm 1.0)$ D (Table 4; Table 2 in Ref. [10]) the upper limit of the interaction elements is $V_0 \cong 0.23$ (± 0.2) eV for all the studied 4-DAAPs in a highly polar environment (*i.e.* in ACN).

It has been shown previously [78] that the appropriate values of the electronic coupling elements V_0, which are mainly determined by the interactions between the atoms forming the D–A bond, can be theoretically predicted following the formalism proposed by Dogonadze et al. [81]. Neglecting contributions from the σ orbitals one can estimate the mutual conformation of the D (dialkylamino group) and A (pyridine ring), *i.e.* the angle $\Theta_{D\text{-}A}$ between the axis perpendicular to the acceptor ring and the axis of the lone pair orbital, l, located on the amino nitrogen N_2:

$$V_0 = C^{D}_{HOMO} C^{A}_{LUMO} \beta_{CN} \cos(\Theta_{D-A}) + const \quad (7)$$

where C^{D}_{HOMO} and C^{A}_{LUMO} are the LCAO coefficients of the $2p_\pi$ atomic orbitals located on the atoms which form the D–A bond (*i.e.* of the l orbital on the adjacent N atom and of the acceptor carbon atom) of the HOMO and LUMO, respectively; β_{CN} is the resonance integral for these atoms, and *const* is related to the electronic interactions between the remaining pairs of atoms in the D–A molecule (this contribution is usually small and negligible due to the fact that β_{CN} is an exponential function of the distance). Very similar values of $C^{D}_{HOMO} = 0.78$ (± 0.04) and $C^{A}_{LUMO} = 0.59$ (± 0.01) were calculated by INDO/S method for the perpendicular conformation of DMAP, MDMAP, TMAP, DEAP and DIAP. Assuming $|\beta_{CN}| = 2.3$ eV [82] and const = 0 one can estimate the angle $\Theta_{D-A} \approx 77(\pm 2)^\circ$. Thus, the analysis of the CT fluorescence of 4-DAAPs under study, similarly to 4-dialkylaminopyrimidines [83], indicates a nearly orthogonal conformation of the most efficiently emitting molecules (*i.e.* related to the maximum of the product of population and the emission rate). The orthogonal conformation of the CT states of these relatively small compounds containing dialkylamino group as an electron donor most probably results from the strong solute-solvent interactions (depending on the magnitude of the ratio μ_e^2/a_0^3) and relatively small effects related to the electronic delocalization from the lone pair orbital on the amino nitrogen to the acceptor ring.

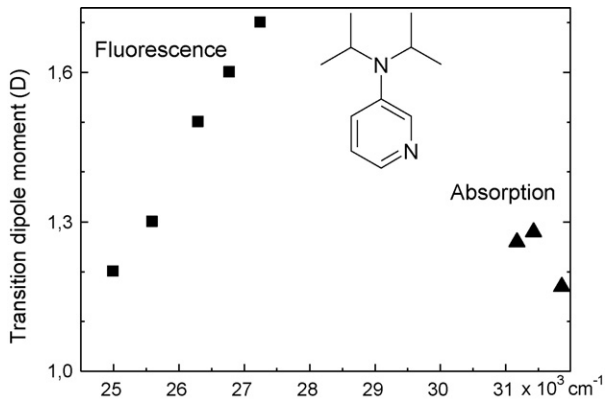

Fig. 5. Correlation between the absorption and fluorescence transition dipole moments and the spectral position of the absorption and fluorescence maxima (expressing the polarity of the surrounding medium) for *m*-DIAP.

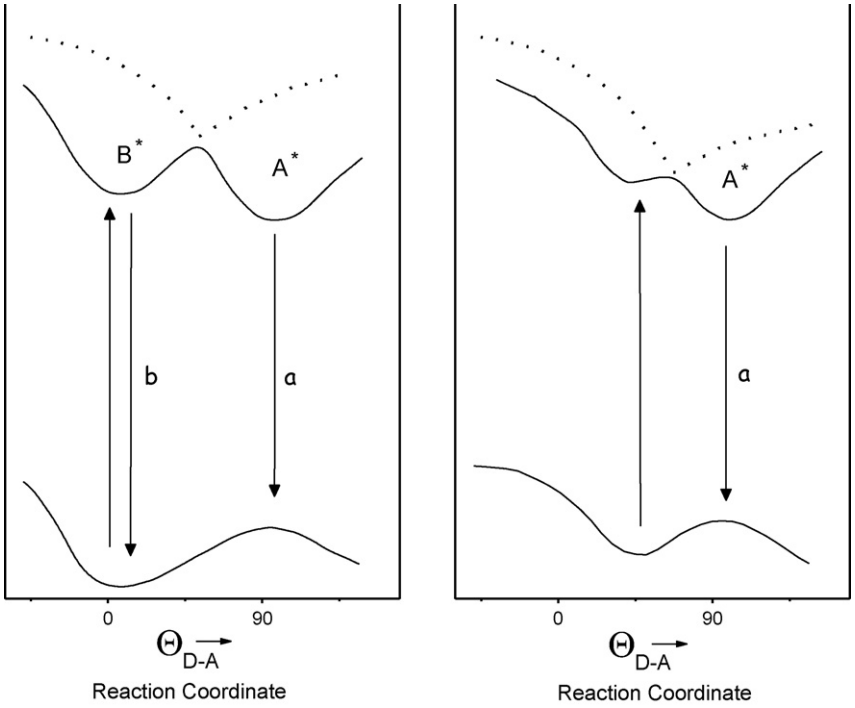

Fig. 6. Schematic kinetic model, in the form of the cross-section of the energy hypersurfaces along the reaction path, represented by torsion around the D–A bond and solvation, for intramolecular ET in 4-dialkylaminopyridines. *Left*, the excited-state energy barrier leads to the dual fluorescence in planar DMAP and DEAP. *Right*, the barrier height is reduced (or cancelled) by large steric repulsions, and only the TICT emission is observed (the case of MDMAP, TMAP and DIAP in polar media).

The radiative properties of *m*-DIAP are different than those of DIAP and other 4-DAAPs. The values of the radiative rate constants k_f of the *meta* isomer are about 4–10 times higher those of the *para* substituted compounds (Table 5). Moreover, Fig. 5 shows the dependence of the values of the electronic transition dipole moments corresponding to fluorescence M_{fl} and absorption M_{abs} on solvent polarity. The M_{abs} values, which are related to the lowest $^1(\pi,\pi^*) \leftarrow S_0$ absorption band, were determined from the approximate expression [73]:

$$\left|\vec{M}_{abs}\right|^2 = \frac{3\ln 10}{8\pi^3 N_A}\frac{hc}{n\tilde{\nu}_{abs}}\int_{band}\varepsilon(\tilde{\nu})d\tilde{\nu}, \quad (8)$$

where $\varepsilon(\tilde{\nu})$ is the molar extinction coefficient at wavenumber $\tilde{\nu}$ and N_A is the Avogadro number.

It should be noted that the M_{fl} values significantly decrease on going from a nonpolar to polar solvent. In the highly polar solvents the values of about 1.2 D are very similar to those of M_{abs} and are about 2 times larger than those of the CT emission of the 4-dialkylaminopyridines. This very interesting result suggests the dependence of the electronic structure and geometry of the fluorescent state of *m*-DIAP on solvent polarity. The higher values of M_{fl} than that of M_{abs} in nonpolar and low-polarity media can be interpreted in terms of the flattening of the molecule upon excitation, whereas in a highly polar environment *m*-DIAP most probably does not undergo any significant conformational changes upon excitation. The electronic structure of the solvent-equilibrated fluorescent state seems to correspond to the $^1(\pi,\pi^*)$ excitation with a charge transfer character depending on the polarity of the solvent. The difference between *m*-DIAP and *para*-substituted dialkylaminopyridines seems to be related to the different shapes of molecular orbitals (Fig. SI1) and, consequently, different interactions between the donor and acceptor subunits.

4. Conclusions

The near-UV electronic absorption and MCD experimental data for DAAPs indicate a presence of three low-energy transitions, assigned to ^1L_b, $^1(n,\pi^*)$ and ^1L_a excited states. These results are corroborated by INDO/S and TD-DFT calculations. It should be noted that, due to the lack of exact C_{2v} symmetry, even in DMAP, the strict distinction between $^1(\pi,\pi^*)$ and $^1(n,\pi^*)$ transitions is not longer possible. The data collected in Tables 3, SI1 and SI2 show a strong mixing between both types of zero-order states, revealed by similar oscillator strengths for "$L_b \leftarrow S_0$" and "$^1(n,\pi^*)$" transitions, as well as by mixed polarization. The transitions polarized along *z*, the long molecular axis, are least perturbed by lowering of symmetry. Naturally, the description in terms of L_b and L_a labels should also be treated as a rather crude approximation. It is thus quite remarkable that the interpretation of the MCD spectra in terms of a simple perimeter model is still possible, even though the presence of a third transition in the low energy region only allows for a qualitative treatment.

The photophysical properties of all the studied 4-DAAPs fit well to the TICT state model (Fig. 6). DMAP and DEAP, the planar compounds in the ground state, show solvent-dependent dual luminescence. The CT emission band is dominant in highly polar solvents such as BN and ACN. The reduction of the energy barrier along the excited-state relaxation path to the TICT state in *ortho*-methylated derivatives (MDMAP and TMAP) and in DIAP by large steric repulsions leads to a single CT fluorescence band in sufficiently polar solvents. The radiative transition in emission $k_f \cong 4 \times 10^6\ s^{-1}$ is forbidden by a factor of 10^{-2} with respect to the value of fully allowed transition as may be expected for a small π-orbital overlap of the nearly orthogonal D–A conformation. The analysis of the transition dipole moments M_{fl} suggests that the geometry of the fluorescent ICT state is close to perpendicular.

Substitution of the amino group at *meta* position in 3-diisopropylaminopyridine (*m*-DIAP) completely changes photophysics: (i) the Franck-Condon excited state initially reached upon excitation and the solvent equilibrated fluorescent state are most probably of the same nature (both excited states do not correspond to a full separation of charges) and (ii) the electronic structure and geometry of the fluorescent CT states of *m*-DIAP are solvent dependent.

Acknowledgements

This work was supported by grant N204 141 32/3545 from the Ministry of Science and Higher Education. The technical assistance of Mrs. Anna Zielińska is greatly appreciated. We thank Prof. Zbigniew R. Grabowski and Prof. Jacek Waluk for stimulating discussions.

Appendix A. Supplementary data

Supplementary data associated with this article can be found, in the online version, at doi:10.1016/j.jphotochem.2009.11.006.

References

[1] E. Lippert, W. Lüder, H. Boss, Fluorescenzspektrum und Franck-Condon-prinzip in lösungen aromatischer verbindungen, in: Advances in Molecular Spectroscopy, Pergamon Press, Oxford, 1962.
[2] Z.R. Grabowski, K. Rotkiewicz, A. Siemiarczuk, D.J. Cowley, W. Baumann, Twisted intramolecular charge transfer states (TICT). A new class of excited states with a full charge separation, Nouv. J. Chim. 3 (1979) 443–454.
[3] Z.R. Grabowski, K. Rotkiewicz, W. Rettig, Structural changes accompanying intramolecular electron transfer: focus on twisted intramolecular charge-transfer states and structures, Chem. Rev. 103 (2003) 3899–4031.
[4] K.A. Zachariasse, Comment on "Pseudo-Jahn-Teller and TICT-models: a photophysical comparison of meta- and para-DMABN derivatives" [Chem. Phys. Lett. 305 (1999) 8]. The PICT model for dual luminescence of aminobenzonitriles, Chem. Phys. Lett. 320 (2000) 8–13.
[5] S. Cogan, S. Zilberg, Y. Haas, The electronic origin of the dual fluorescence in donor–acceptor substituted benzene derivatives, J. Am. Chem. Soc. 128 (2006) 3335–3345.
[6] R. Czerwieniec, J. Herbich, A. Kapturkiewicz, J. Nowacki, Radiative electron transfer in planar donor–acceptor quinoxaline derivatives, Chem. Phys. Lett. 325 (2000) 589–598.
[7] J. Herbich, J. Waluk, Excited charge transfer states in 4-aminopyrimidines, 4-(dimetylanilino)pyrimidine and 4-(dimethylamino)pyridine, Chem. Phys. 188 (1994) 247–265.
[8] C. Cazeau-Dubroca, G. Nouchi, M. Ben Brahim, M. Pesquer, D. Gorse, P. Cazeau, Dual fluorescence of 4-N,N-dimethylaminopyridine. Role of hydrogen-bonded complex in the ground state, J. Photochem. Photobiol. A: Chem. 80 (1994) 125–133.
[9] S. Mishina, M. Takayanagi, M. Nakata, J. Otsuki, K. Araki, Dual fluorescence of 4-dimethylaminopyridine and its derivatives. Effects of methyl substitution at the pyridine ring, J. Photochem. Photobiol. A: Chem. 141 (2001) 153–158.
[10] I. Szydłowska, A. Kyrychenko, J. Nowacki, J. Herbich, Photoinduced intramolecular electron transfer in 4-dimethylaminopyridines, Phys. Chem. Chem. Phys. 5 (2003) 1032–1038.
[11] I. Szydłowska, A. Kyrychenko, A. Gorski, J. Waluk, J. Herbich, Excited states of 4-dimethylaminopyridines: magnetic circular dichroism and computational studies, Photochem. Photobiol. Sci. 2 (2003) 187–194.
[12] I. Szydłowska, J. Kubicki, J. Herbich, Picosecond kinetics of excited-state charge separation in 4-(dimethylamino)pyridine, Photochem. Photobiol. Sci. 4 (2005) 106–112.
[13] I. Szydłowska, J. Nowacki, A. Zielińska, J. Herbich, Hydrogen bonding and protonation effects on excited-state electron transfer in *meta*- and *para*-dialkylaminopyridines, Pol. J. Chem. 82 (2008) 847–864.
[14] G. Höfle, W. Steglich, H. Vorbrüggen, 4-Dialkylaminopyridines as highly active acylation catalysts [New synthetic method (25)], Angew. Chem. Int. Ed. 17 (1978) 569–583.
[15] E.F.V. Scriven, 4-Dialkylaminopyridines: super acylation and alkylation catalysts, Chem. Soc. Rev. 12 (1983) 129–161.
[16] D.I. Gittings, F. Caruso, Spontaneous phase transfer of nanoparticulate metals from organic to aqueous media, Angew. Chem. Int. Ed. 40 (2001) 3001–3004.
[17] V.J. Gandubert, R.B. Lennox, Assessment of 4-(dimethylamino)pyridine as a capping agent for gold nanoparticles, Langmuir 21 (2005) 6532–6539.

[18] M.-C. Daniel, D. Astruc, Gold nanoparticles: assembly, supramolecular chemistry, quantum-size-related properties, and applications toward biology, catalysis and nanotechnology, Chem. Rev. 104 (2004) 293–346.
[19] C.M. McIntosh, E.A. Esposito, A.K. Boal, J.M. Simard, C.T. Martin, V.M. Rotello, Inhibition of DNA transcription using cationic mixed monolayer protected gold clusters, J. Am. Chem. Soc. 123 (2001) 7626–7629.
[20] D.J. Maxwell, J.R. Taylor, S. Nie, Self-assembled nanoparticle probes for recognition and detection of biomolecules, J. Am. Chem. Soc. 124 (2002) 9606–9612.
[21] R. Llinás, K. Walton, V. Bohr, Synaptic transmission in squid giant synapse after potassium conductance blockage with external 3- and 4-aminopyridine, Biophys. J. 16 (1976) 83–86.
[22] D. Agoston, P. Hargittai, A. Nagy, Effects of a 4-aminopyridine in calcium movements and changes of membrane potential in pinched-off nerve terminals from rat cerebral cortex, J. Neurochem. 41 (1983) 745.
[23] A. Weisstuch, A.C. Testa, A fluorescence study of aminopyridines, J. Phys. Chem. 72 (1968) 1982–1987.
[24] A. Weisstuch, A.C. Testa, Fluorescence study of 2-(N,N-dimethylamino)pyridine and related molecules, J. Phys. Chem. 74 (1970) 2299–2303.
[25] S. Babiak, A.C. Testa, Fluorescence lifetime study of aminopyridines, J. Phys. Chem. 80 (1976) 1882–1885.
[26] W. Rettig, B. Bliss, K. Dirnberger, Pseudo-Jahn-Teller and TICT-models: a photophysical comparison of *meta*- and *para*-DMABN derivatives, Chem. Phys. Lett. 305 (1999) 8–14.
[27] S. Murali, W. Rettig, TICT formation in para- and meta-derivatives of N-phenylpyrrole, J. Phys. Chem. A 110 (2006) 28–37.
[28] J.M. Essery, K. Schofield, Some derivatives of 4-amino- and 4-nitro-pyridine, Chem. Soc. (1960) 4953–4959.
[29] T. Kauffman, R. Nürnberg, Zur konkurrenz des eliminierungs-additions- und additions-eliminierungs-mechanismus bei nucleophilen substitutionsreaktionen an 4-halogen pyridinen, Chem. Ber. 100 (1967) 3427–3431.
[30] E.B. Pedersen, D. Carlsen, Phosphoramides: VIII. Phosphorus pentoxide/amine mixtures as reagents in a facile synthesis of dialkylaminopyridines, Synthesis (1978) 844–845.
[31] K. Vinter-Pasquier, B. Jamart-Grégoire, P. Caubère, Complex base-induced generation of 3,4-didehydropyridine derivatives: new access to aminopyridines or pyridones, Heterocycles 45 (1997) 2113–2129.
[32] C. Reihardt, Solvent Effects in Organic Chemistry, Monographs in Modern Chemistry, Vol. 3, VCH Weinheim, New York, 1979.
[33] J. Jasny, Multifunctional spectrofluorimetric system, J. Lumin. 17 (1978) 149–173.
[34] R.A. Velapoldi, Considerations on organic compounds in solution and inorganic ions in glasses as fluorescent standard reference materials, in: Proc. Conf. NBS, National Bureau of Standards, Gaithersburg, MD, 1972, p. 231.
[35] A. Gorski, E. Vogel, J.L. Sessler, J. Waluk, Magnetic circular dichroism of neutral and ionic forms of octaethylhemiporphycene, Chem. Phys. 282 (2002) 37–49.
[36] M.J. Frisch, G.W. Trucks, H.B. Schlegel, G.E. Scuseria, M.A. Robb, J.R. Cheeseman, V.G. Zakrzewski, J.J.A. Montgomery, R.E. Stratman, J.C. Burant, S. Dapprich, J.M. Millam, A.D. Daniels, K.N. Kudin, M.C. Strain, O. Farkas, J. Tomasi, V. Barone, M. Cossi, R. Cammi, B. Mennucci, C. Pomelli, C. Adamo, S. Clifford, J. Ochterski, G.A. Petersson, P.Y. Ayala, Q. Cui, K. Morokuma, D.K. Malick, A.D. Rabuck, K. Raghavachari, J.B. Foresman, J. Cioslowski, J.V. Ortiz, A.G. Baboul, B.B. Stefanov, G. Liu, A. Liashenko, P. Piskorz, I. Komaromi, R. Gomperts, R.L. Martin, D.J. Fox, T. Keith, M.A. Al-Laham, C.Y. Peng, A. Nanayakkara, C. Gonzalez, M. Challacombe, P.M.W. Gill, B. Johnson, W. Chen, M.W. Wong, J.L. Andres, C. Gonzales, M. Head-Gordon, E.S. Replogle, J.A. Pople, GAUSSIAN 98, revision A.7, Gaussian, Inc., Pittsburgh, PA, 1998.
[37] M.J. Frisch, G.W. Trucks, H.B. Schlegel, G.E. Scuseria, M.A. Robb, J.R. Cheeseman, J.J.A. Montgomery, T. Vreven, K.N. Kudin, J.C. Burant, J.M. Millam, S.S. Iyengar, J. Tomasi, V. Barone, B. Mennucci, M. Cossi, G. Scalmani, N. Rega, G.A. Petersson, H. Nakatsuji, M. Hada, M. Ehara, K. Toyota, R. Fukada, J. Hasegawa, M. Ishida, T. Nakajima, Y. Honda, O. Kitao, H. Nakai, M. Klene, X. Li, J.E. Knox, H.P. Hratchian, J.B. Cross, C. Amado, J. Jaramillo, R. Gomperts, R.E. Stratmann, O. Yazyev, A.J. Austin, R. Cammi, C. Pomelli, J. Ochterski, P.Y. Ayala, K. Morokuma, G.A. Voth, P. Salvador, J.J. Donnenberg, V.G. Zakrzewski, S. Dapprich, A.D. Daniels, M.C. Strain, O. Farkas, D.K. Malick, A.D. Rabuck, K. Raghavachari, J.B. Foresman, J.V. Ortiz, Q. Cui, A.G. Baboul, S. Clifford, J. Cioslowski, B.B. Stefanov, G. Liu, A. Liashenko, P. Piskorz, I. Komaromi, R.L. Martin, D.J. Fox, T. Keith, M.A. Al-Laham, C.Y. Peng, A. Nanayakkara, M. Challacombe, P.M.W. Gill, B. Johnson, W. Chen, M.W. Wong, C. Gonzales, J.A. Pople, GAUSSIAN 03, revision C.02, Gaussian, Inc., Wallingford CT, 2004.
[38] W. Kohn, L.J. Sham, Self-consistent equations including exchange and correlation effects, Phys. Rev. 140 (1965) A1133–A1138.
[39] R.G. Parr, W. Yang, Density-Functional Theory of Atoms and Molecules, Oxford University Press, Oxford, 1988.
[40] A.D. Becke, Density functional exchange approximation with correct asymptotic behavior, Phys. Rev. A 38 (1988) 3098–3100.
[41] C. Lee, W. Yang, R.G. Parr, Development of the Colle-Salvetti correlation-energy formula into a functional of the electron density, Phys. Rev. B 37 (1988) 785–789.
[42] R.E. Stratmann, G.E. Scuseria, M.J. Frisch, An efficient instrumentation of time-dependent density functional theory for the calculation of excitation energies of large molecules, J. Chem. Phys. 109 (1998) 8218–8224.
[43] S. Miertus, E. Scrocco, J. Tomasi, Electrostatic interactions of a solute with a continuum. A direct utilization of ab initio molecular potentials for the prevision of solvent effect, Chem. Phys. 55 (1981) 117–129.
[44] J.E. Ridley, M.C. Zerner, An intermediate neglect of differential overlap technique for spectroscopy: pyrrole and the azines, Theor. Chim. Acta 32 (1973) 111–134.
[45] U. Ohms, H. Guth, Die Kristall- und Molekulstruktur von 4-Dimethylaminopyridin $C_7H_{10}N_2$, Z. Kristallogr. 166 (1984) 213–217.
[46] A.B.J. Parusel, G. Köhler, Influence of the alkyl chain length on the excited-state properties of 4-dialkyl-benzonitriles. A theoretical DFT/MRCI study, Int. J. Quantum Chem. 84 (2001) 149–156.
[47] W. Rettig, R. Gleiter, Dependence of intramolecular rotation in p-cyano-N,N-dialkylanilines on the twist angle. A fluorescence, UV absorption, and photoelectron spectroscopic studies, J. Phys. Chem. 89 (1985) 4676–4680.
[48] W.M. Kwok, C. Ma, P. Matousek, A.W. Parker, D. Philips, W.T. Toner, M. Towrie, P. Zuo, D.L. Philips, Time-resolved spectroscopy study of the triplet state of 4-diethylaminobenzonitrile (DEABN), Phys. Chem. Chem. Phys. 5 (2003) 3643–3652.
[49] S. Techert, K.A. Zachariasse, Structure determination of the intramolecular charge transfer state in crystalline 4-(diisopropylamino)benzonitrile from picosecond X-ray diffraction, J. Am. Chem. Soc. 126 (2004) 5593–5600.
[50] A. Demeter, S. Druzhinin, M. George, E. Haselbach, J.L. Roulin, K.A. Zachariasse, Dual fluorescence and fast intramolecular charge transfer with 4-(diisopropylamino)benzonitrile in alkane solvents, Chem. Phys. Lett. 323 (2000) 351–360.
[51] A. Castellan, J. Michl, Magnetic circular dichroism of cyclic π-electron systems. 4. Aza analogues of benzene, J. Am. Chem. Soc. 100 (1978) 6824–6827.
[52] J. Michl, Magnetic circular dichroism of aromatic molecules, Tetrahedron 40 (1984) 3845–3934.
[53] S.L. Wallace, A. Castellan, D. Muller, J. Michl, Magnetic circular dichroism of cyclic π-electron systems. 5. Derivatives of pyridine, J. Am. Chem. Soc. 100 (1978) 6828–6834.
[54] M. Vašák, J.W. Downing, L.B. Townsed, J. Michl, Magnetic circular dichroism of cyclic π-electron systems. 25. Oxo-derivatives of indazole, benzimidazole and purine, Tetrahedron 38 (1982) 1571–1578.
[55] Y.N. Svartsov, Photophysics of aminosubstituted phthalides, Ph.D. Thesis, Institute of Physical Chemistry Polish Academy of Sciences, Warsaw, Poland, 2006.
[56] K. Rotkiewicz, Z.R. Grabowski, A. Krówczyński, W. Kühnle, Picosecond chemical relaxation of excited *p*-cyano-N,N-dialkylanilines, J. Lumin. 12/13 (1976) 877–885.
[57] G. Köhler, N. Getoff, K. Rotkiewicz, Z.R. Grabowski, Electron photoejection from donor-aryl-acceptor molecules in aqueous solution, J. Photochem. 28 (1985) 537.
[58] R.A. Marcus, Relation between charge transfer absorption and fluorescence spectra and the inverted region, J. Phys. Chem. 93 (1989) 3078–3086.
[59] I. Franssen Szydłowska, Y. Nosenko, B. Brutschy, J. Herbich, Dual fluorescence of 4-dialkylaminopyridines under supersonic jet conditions, Chem. Phys. Lett. 467 (2008) 58–65.
[60] W. Schuddeboom, S.A. Jonker, J.M. Warman, U. Leinhos, W. Kühnle, K.A. Zachariasse, Excited-state dipole moments of dual fluorescent 4-(dialkylamino)benzonitriles. Influence of alkyl chain length and effective solvent polarity, J. Phys. Chem. 96 (1992) 10809–10819.
[61] K.A. Zachariasse, M. Grobys, Th. von der Haar, A. Hebecker, Yu.V. Il'ichev, Y.B. Jiang, O. Morawski, W. Kühnle, Intramolecular charge transfer in the excited state. Kinetics and configurational changes, J. Photochem. Photobiol. A: Chem. 102 (1996) 59–70.
[62] Y.V. Il'ichev, W. Kühnle, K.A. Zachariasse, Intramolecular charge transfer in dual fluorescent 4-(dialkylamino)benzonitriles. Reaction efficiency enhancement by increasing the size of the amino and benzonitrile subunits by alkyl substituents, J. Phys. Chem. A 102 (1998) 5670–5680.
[63] J. Herbich, Z.R. Grabowski, H. Wójtowicz, H. Golankiewicz, Dual fluorescence of 4-(dialkylamino)pyrimidines. Twisted intramolecular charge transfer state formation favored by hydrogen bond or by coordination to the metal ion, J. Phys. Chem. 93 (1989) 3439–3444.
[64] E. Lippert, Dipolmoment und elektronenstruktur von angeregten molekülen, Z. Naturforsch. 10A (1955) 541–545.
[65] N. Mataga, Y. Kaifu, M. Koizumi, Solvent effects upon fluorescence spectra and the dipole moments of excited molecules, Bull. Chem. Soc. Jpn. 29 (1956) 465–470.
[66] L. Onsager, Electric moments of molecules in liquids, J. Am. Chem. Soc. 58 (1936) 1486–1493.
[67] E. Litońska, Z. Proba, I. Kułakowska, K.L. Wierzchowski, Conformation of the $N(CH_3)_2$ group in cytosine and in simple model pyrimidines and pyridines. Steric effects of ortho-methyl substitution on infrared spectra and molecular dipole moments, Acta Biochim. Polon. 26 (1979) 39–54.
[68] E.C. Lim, Vibronic interactions and luminescence in aromatic molecules with nonbonding electrons, in: E.C. Lim (Ed.), Excited States, vol. 3, Academic Press, New York, 1977, pp. 305–337.
[69] A.C. Testa, Triplet–triplet absorption in 4-N-dimethylaminopyridine, J. Chem. Phys. 57 (1972) 3019–3020.
[70] A.C. Testa, Flash photolysis study of 4-N-dimethylaminopyridine, J. Am. Chem. Soc. 95 (1973) 3128–3131.
[71] A. Demeter, V. Mile, T. Bérces, Hydrogen bond formation between 4-(dimethylamino)pyridine and aliphatic alcohols, J. Phys. Chem. A 111 (2007) 8942–8949.
[72] J.B. Birks, Photophysics of Aromatic Molecules, Wiley, New York, 1978.
[73] J. Michl, E.W. Thulstrup, Spectroscopy with Polarized Light, Wiley, New York, 1986.

[74] R.S. Mulliken, Molecular compounds and their spectra. II, J. Am. Chem. Soc. 74 (1952) 811–824.
[75] R.S. Mulliken, W.B. Person, Molecular Complexes: A Lecture and Reprint Volume, Wiley, New York, 1969.
[76] J.N. Murrell, Molecular complexes and their spectra. IX. The relationship between the stability of the complex and the intensity of its charge-transfer bands, J. Am. Chem. Soc. 81 (1959) 5037–5043.
[77] M. Bixon, J. Jortner, J.W. Verhoeven, Lifetimes for radiative charge recombination in donor–acceptor molecules, J. Am. Chem. Soc. 116 (1994) 7349–7355.
[78] A. Kapturkiewicz, J. Herbich, J. Karpiuk, J. Nowacki, Intramolecular radiative and radiationless charge recombination processes in donor–acceptor carbazole derivatives, J. Phys. Chem. A 101 (1997) 2332–2344.
[79] J. Herbich, A. Kapturkiewicz, Electronic structure and molecular conformation in the excited charge transfer singlet states of 9-acridyl and other aryl derivatives of aromatic amines, J. Am. Chem. Soc. 120 (1998) 1014–1029.
[80] K.K. Innes, I.G. Ross, W.R. Moomaw, Electronic states of azabenzenes and azanaphthalenes: a revised and extended critical review, J. Mol. Spectr. 132 (1988) 492–544.
[81] R.R. Dogonadze, A.M. Kuznetsov, T. Marsagishvili, The present state of the theory of charge transfer processes in condensed phase, Electrochim. Acta 25 (1980) 1–28.
[82] F.P. Billingsley, J.E. Bloor, Theoretical studies on the electronic spectra of substituted aromatic molecules. IV. PPP-SCF parameters for polysubstituted benzenes and five-membered ring heterocyclics containing nitrogen, oxygen and sulfur, Theor. Chim. Acta 11 (1968) 325–343.
[83] J. Herbich, B. Brutschy, TICT molecules, in: V. Balzani (Ed.), Electron Transfer in Chemistry, vol. 4, Wiley VCH, Weinheim, 2001, pp. 697–741.